AFCRL-

Influence of Particle Size Distribution on Reflected and Transmitted Light from Clouds

Authors

George W. Kattawar
Gilbert N. Plass

Southwest Center for Advanced Studies
Dallas, Texas

Contract No. AF19(628)-5039

Project No. 4076

Task No. 407604

NSR-269 & NAR-44-004 026

Scientific Report No. 5

24 August 1967

This research was partially supported by the National Aeronautics and Space Administration

Contract Monitor
Robert W. Fenn
Optical Physics Laboratory

Prepared
for

AIR FORCE CAMBRIDGE RESEARCH LABORATORIES
OFFICE OF AEROSPACE RESEARCH
UNITED STATES AIR FORCE
BEDFORD, MASSACHUSETTS 01730

AFCRL-

Influence of Particle Size Distribution on Reflected and Transmitted Light from Clouds

Authors

George W. Kattawar
Gilbert N. Plass

Southwest Center for Advanced Studies
Dallas, Texas

Contract No. AF19(628)-5039

Project No. 4076

Task No. 407604

Scientific Report No. 5

24 August 1967

This research was partially supported by the National Aeronautics and Space Administration

Contract Monitor
Robert W. Fenn
Optical Physics Laboratory

Prepared
for

AIR FORCE CAMBRIDGE RESEARCH LABORATORIES
OFFICE OF AEROSPACE RESEARCH
UNITED STATES AIR FORCE
BEDFORD, MASSACHUSETTS 01730

Influence of Particle Size Distribution on Reflected and Transmitted Light from Clouds

GEORGE W. KATTAWAR and GILBERT N. PLASS

Abstract

The light reflected and transmitted from clouds with various drop size distributions is calculated by a Monte Carlo technique. Six different models are used for the drop size distribution: isotropic, Rayleigh; haze continental; haze maritime; cumulus; nimbostratus. The scattering function for each model is calculated from the Mie theory. In general the reflected and transmitted radiances for the isotropic and Rayleigh models tend to be similar as are those for the various haze and cloud models. The reflected radiance is less for the haze and cloud models than for the isotropic and Rayleigh models, except for an angle of incidence near the horizon when it is larger around the incident beam direction. The transmitted radiance is always much larger for the haze and cloud models near the incident direction; at distant angles it is less for small and moderate optical thicknesses and greater for large optical thicknesses (all comparisons to isotropic and Rayleigh models). The downward flux, cloud albedo, and mean optical path are discussed. The angular spread of the beam as a function of optical thickness is shown for the nimbostratus model.

George W. Kattawar is with North Texas State University, Denton, Texas 76203. Gilbert N. Plass is with the Southwest Center for Advanced Studies, P. O. Box 30365, Dallas, Texas 75230.

Introduction

The distribution of light reflected and transmitted by a cloud depends on the number and size distribution of the water droplets, the wavelength of the light, the single scattering albedo, the albedo of the planetary surface, the angle of the incoming solar radiation, and the optical thickness of the cloud together with its shape. We have described in the literature[1] a computer program which calculates the reflected and transmitted radiance by the Monte Carlo method. The path of the photon is accurately followed in three-dimensions. A single scattering phase function is obtained from the Mie theory by integration over the particle size distribution. The probability of scattering at any angle is accurately calculated including the strong forward peak of the distribution. Thus the calculation simulates accurately the numerous small angle collisions which occur.

The Monte Carlo method appears to offer the only practical way to make calculations for real planetary atmospheres where the occurrence of such effects as strong forward scattering, inhomogeneities in the atmosphere, emission, non-Lambertian reflecting surfaces, and a number of different processes which absorb, scatter, and reemit the photon may profoundly influence the results. Fritz[2,3] and Twomey et al[4] have calculated the effects of light scattering from clouds by other methods and have obtained very interesting results. The Monte Carlo method has been discussed by Hammersley and Handscomb[5] and has been applied to atmospheric problems by Collins and Wells[6]. Twomey et al[4] have given the variation in the magnitude of the diffuse reflection for various Gaussian size distributions with different average radii

and standard deviations. However, no one has attempted to evaluate the influence of various size distributions of different shapes on both the reflected and transmitted light.

Cloud Models

Six different phase functions were chosen for this calculation in order to span the various distributions which occur in actual clouds. These phase functions are named isotropic, Rayleigh, haze continental (haze C), haze maritime (haze M), cumulus, and nimbostratus. The isotropic phase function is, of course, independent of angle. Although it does not correspond to any physical situation, it is useful to have for comparison with the other models. The Rayleigh phase function is applicable when the radius of all the scattering particles is considerably smaller than the wavelength.

The next three models are taken from Deirmendjian[7]. The haze C model is defined by the equation

$$n(r) = \begin{cases} 0, & r < 0.03\mu \\ 10^3, & 0.03\mu < r < 0.1 \\ 0.1r^{-4}, & r > 0.1\mu, \end{cases} \qquad (1)$$

where r is the radius in microns and n(r) is the particle concentration in $cm^{-3}\mu^{-1}$. This corresponds to a continental haze with the typical r^{-4} variation in the number of particles.

The haze M model is defined by the equation

$$n(r) = 5.33 \times 10^4 r \exp(-8.944 r^{\frac{1}{2}}) \qquad (2)$$

and corresponds to a maritime haze with the maximum number of particles at $r = 0.71\mu$.

The cumulus cloud model assumes that

$$n(r) = 2.373\, r^6 \exp(-1.5r). \tag{3}$$

The maximum particle concentration occurs when $r = 4\mu$.

The nimbostratus cloud model assumes that

$$n(r) = 0.00108\, r^6 \exp(-0.5r). \tag{4}$$

The maximum particle concentration occurs when $r = 12\mu$. This distribution approximately represents rather divergent measurements[8,9] which have been made for nimbostratus clouds. In any case this distribution is representative of clouds with substantial numbers of larger droplets. The constant in Eqs. (1-4) is proportional to the total number of particles per unit volume. Since all results in this paper are presented in terms of optical depth the values chosen for these constants are immaterial; they are only needed for the conversion of optical depth to an actual height.

The single scattering phase function was calculated for the four particle distributions represented by Eqs. (1-4) from the Mie theory.[10] In each case the range of integration was partitioned into many sub-intervals in each of which third order Gauss quadrature was applied. A wavelength λ of 0.7μ for the incident light and a real index of refraction of 1.33 for the water droplets was assumed for this calculation. The single scattering phase function was calculated at 0.25° intervals in the forward directions near the strong forward scattering maximum and at 2° intervals in the backward direction where the function

undergoes several oscillations. The results are shown in Figure 1 together with the well known results for the Rayleigh and isotropic phase functions. The insets in the upper portions of the figure show the curves in more detail in the regions near a scattering angle $\Theta = 0$ and π.

The cumulative probability for scattering as a function of angle was obtained for each distribution by accurate numerical integration. The accuracy was checked by integration over the unit sphere and was always within a few hundredths of one percent of unity.

All calculations reported here assume a single scattering albedo ω_o of unity and reflection from a Lambert's surface as representative of the planetary surface. Results are reported for a surface albedo A of 0 and 1. The incident flux is normalized to unity (instead of the value π sometimes chosen).

Reflected Radiance

The reflected radiance was calculated for each of these six particle distribution functions by the Monte Carlo method[1]. Although results are available for the isotropic and Rayleigh functions for atmospheres of finite thickness, the radiances were also calculated for these cases by the Monte Carlo method in order to have results averaged over the same combination of zenith and azimuthal angles as for the other distribution functions.

The reflected radiance for vertically incident sunlight ($\mu_o = -1$) is shown in Figures 2-4 for $\tau = 0.01$, 1, and 10. When $\mu_o = -1$ the reflected radiance depends only on the scattering function from $\Theta = \frac{1}{2}\pi$ to π.

For small optical depths and surface albedo A = 0, the reflected radiance is proportional to the scattering function divided by the cosine of the zenith angle. The reflected radiance calculated in this manner for single scattering and for $\tau = 0.01$ is shown in Figure 2 by small squares. These values calculated for single scattering agree well with the Monte Carlo results except near the horizon where multiple scattering influences the result. The correspondence of the reflected radiance with the scattering function is shown for example in the peak in the radiance value for the nimbostratus model in the interval of μ from 0.7 to 0.8; this corresponds directly to the peak in the scattering function at $\cos \Theta = -0.77$ shown in Figure 1. When A = 1, the reflected radiance is virtually independent of μ. For a thin cloud the uniformly reflected radiation from the planetary surface is not appreciably modified by the cloud.

When $\tau = 1$, the reflected radiance is shown in Figure 3. When A = 0, there is relatively little variation with μ for isotropic and Rayleigh scattering. The reflected radiance is considerably less for the haze and cloud models and it exhibits more angular variation. In general, the radiance decreases at each angle as the forward scattering of the cloud particles increases. When A = 1, the reflected radiance increases monotonically as μ increases in all models.

The reflected radiance for $\tau = 10$ is shown in Figure 4. Although the differences between the various models are less for this thick cloud than they were for thinner clouds, they are still appreciable. The curves for the haze and cloud models show considerable angular variation and have a maximum near, but not at the zenith when A = 0.

When A = 1, the curves for the different models are quite close together near the zenith, but depart from each other near the horizon. It is interesting that such appreciable differences develop for thick clouds between models. These differences result from the high probability for small angle scattering on the first collision for the haze and cloud models. When the forward scattering is quite strong successive collisions of the photons occur at a greater average depth and thus fewer photons can escape back out of the cloud top.

The reflected radiance when the incident sunlight is near the horizon ($\mu_o = -0.1$) is shown in Figures 5-8. Figure 5 is for the case $\tau = 0.01$ and A = 0. The values have been averaged over the azimuthal angle for 90° on both sides of the original beam. The values on the left side of the graph include the angles closest to the original beam direction. Thus the reflected radiances are higher in general on the left side than are the corresponding values on the right side, since the scattering function for Mie particles is larger in general in the forward hemisphere than at corresponding angles in the backward hemisphere.

For the angles closest to the direction of the original beam ($0 < \mu < 0.1$ on left side of Figure 5) the isotropic and Rayleigh reflected radiances are the lowest of the various models because of the high probability of small angle forward scattering by the Mie particles. On the other hand the isotropic and Rayleigh reflected radiances are the highest in the direction farthest from the original beam ($0 < \mu < 0.1$ on the right side of Figure 5) because of the small probability of backward scattering by Mie particles. When $\mu_o = -0.1$,

there is only an approximate correlation between the reflected radiance as a function of the cosine of the viewing angle μ and the scattering function as a function of the scattering angle Θ. This is because the scattering function must be averaged over all appropriate azimuthal angles. For example, for the range $0 < \mu < 0.1$ on the left side of Figure 5, the scattering angle Θ varies between 10° and 90° as the azimuthal angle changes.

Near the zenith there is relatively little change in Θ as the azimuthal angles varies, so that the reflected radiance is rather closely proportional to the scattering function. The nimbostratus model has the lowest radiance values of any model near the zenith and on the entire right side of the figure. The reflected radiance for this model is 2000 times less near the zenith than at the near horizon. The curves for $\tau = 0.01$ and $A = 1$ (not shown here) are essentially constant except for approximately a two-fold rise in the radiance of the Mie models on the near horizon and a slight rise of the isotropic and Rayleigh models on both horizons.

The reflected radiance for $\tau \blacksquare 1$, $\mu_o = -0.1$ and $A = 0$ is given in Figure 6. These curves are very similar to those for $\tau \blacksquare 0.01$; the radiance values are greater and the differences between the curves for the different models is smaller when $\tau \blacksquare 1$ than when $\tau = 0.01$ because of the greater multiple scattering in the former case. The curves in Figure 6 divide into two groups with relatively small differences between them: the isotropic and Rayleigh models on the one hand and the

haze and cloud models on the other hand. The haze and cloud models give a larger radiance on the near horizon and a smaller radiance at other angles than the isotropic and Rayleigh models. The reflected radiance for the nimbostratus model is 170 times larger on the near horizon than at the zenith.

When $A = 1$ and $\tau = 1$, the curves are shown in Figure 7. Again they divide into two groups as before with the same qualitative behavior. The magnitude of the variation is less than for $A = 0$ since the reflected radiation from the planetary surface tends to smooth the curves when $A = 1$.

The curves for $\tau = 10$ and $A = 0$ are shown in Figure 8. Once again the curves divide into two groups and are qualitatively similar to those for $\tau = 1$, but with a smaller variation in the functions. There is somewhat more fluctuation in the Monte Carlo results for $\tau = 10$ than in the previous results, since a smaller number of photons were followed in the computations for large τ. There is still a 34 fold variation in the reflected radiance for the nimbostratus model between the near horizon and the zenith. A study of the reflected radiation from a cloud that has a large optical thickness with light incident at this angle can easily determine whether Rayleigh or Mie particles are the scattering centers. If the scattering centers are Mie particles, there is considerable asymmetry in the reflected radiance between the near and far horizons. The curves are not changed appreciably in shape and the values are only slightly increased when $A = 1$.

Transmitted Radiance

The transmitted radiance when the sun is at the zenith is shown in Figures 9-11. For an optically thin cloud ($\tau = 0.01$) and $A = 0$, the transmitted radiance is closely proportional to the scattering function divided by μ (except at the zenith where the value is increased by multiple scattering). Values calculated in this manner are indicated by small squares in Figure 9. These single scattering values agree well with the Monte Carlo results except near the zenith where small angle multiple scattering is important. A comparison of these results gives an indication of the fluctuations in the Monte Carlo results. The haze and cloud models have considerably larger radiances near the zenith than the isotropic and Rayleigh models because of the large forward scattering by Mie particles. On the other hand the haze and cloud models have smaller radiance values near the horizon because of the smaller probability for scattering from Mie particles through angles near 90° than from an isotropic or Rayleigh distribution.

The curves for an optically thin cloud are considerably modified when $A = 1$ by the reflected radiation from the planetary surface. In this case the radiance is greater at the horizon than at the zenith when averaged over μ intervals of 0.1.

The results for a cloud of intermediate optical thickness ($\tau = 1$) and $\mu_o = -1$ are shown in Figure 10. When these curves are compared with Figure 9, the effects of multiple scattering are evident in reducing the value at the horizon compared to the value at the zenith. The isotropic and Rayleigh radiances show only small variations with μ,

while those for the haze and cloud models all show a minimum at the horizon with a steep rise to a maximum at the zenith. The radiance is largest at the zenith for the nimbostratus and cumulus models because of their large forward scattering functions. The modification in these curves when A = 1 is also shown in Figure 10.

When the cloud is optically thick (τ = 10), the transmitted radiance is shown in Figure 11. All of the radiance values for A = 0 increase from the horizon to the zenith; the values for the haze and cloud models are approximately three times larger at the zenith than at the horizon. Unfortunately the values from μ = 0 to 0.1 in this case have a relatively large statistical fluctuation. This is because of the small number of photons which penetrate such an optically thick cloud and leave the lower surface at an angle near the horizon. Many fewer photons penetrate a thick cloud for the isotropic and Rayleigh models than for the haze and cloud models; thus the fluctuations are particularly large in the former case. When A = 1 the transmitted radiance exhibits relatively little variation with angle or between models.

The results when μ_o = -0.1 are shown in Figures 12-15. When the cloud is optically thin (τ = 0.01), the transmitted radiance can be obtained directly from the scattering functions for the various models, except for multiple scattering effects near the original beam direction. Allowance must be made for the various scattering angles which occur as the azimuthal angle varies over all possible values appropriate for the averaged results shown. The transmitted radiance near the direction of the original beam is considerably larger for the haze and cloud models than for the isotropic and Rayleigh models. This is because of

the numerous, probable small angle scattering events in the former case. On the other hand the radiance is less for the haze and cloud models near the zenith and toward the far horizon. The curves for A = 0 are shown here as they are qualitatively similar and only slightly higher. The greatest increase with surface albedo is near the zenith direction where the radiance values are low when A = 0.

The curves for an intermediate optical depth (τ = 1) and A = 0 are shown in Figure 13. The maximum radiance for the haze and cloud models is no longer in the original beam direction, but has moved closer to the zenith; the minimum radiance for the same models occurs just beyond the zenith on the side away from the original beam direction. The radiance for the haze and cloud models is appreciably larger than that for the isotropic and Rayleigh models from the near horizon almost to the zenith; the opposite is true from the zenith to the far horizon. The results for A ▫ 1 are shown in Figure 14. The radiance values are somewhat larger than in Figure 13, but the same qualitative relationships are still valid.

The radiance when the optical thickness is large (τ ▫ 10) is given in Figure 15 for A ▫ 0. The values near the horizon have a greater statistical fluctuation than do other values in this or other figures shown here. An analysis shows that a few improbable events contribute most of the radiance near the horizon; thus if these events do not occur by chance in a particular calculation, the radiance value is too low. The most striking result shown here is that the radiance values at all angles are lower for the isotropic and Rayleigh models

than for the haze and cumulus models. The reason for this is that more photons can penetrate deeper into the cloud when there is strong forward scattering than when the scattering is more nearly isotropic. The largest radiance values occur for the nimbostratus model which has the sharpest forward scattering function. The maximum for all models is now nearer the zenith than the incident direction.

Between 150,000 and 200,000 photon collisions were calculated for a typical curve shown here. The smallest and largest number of photon collisions calculated were both for the Rayleigh model: 83,405 collisions when $\tau = 0.01$ and $\mu_o = -1$ and 899,858 collisions when $\tau = 1$ and $\mu_o = -1$. In a typical run 30,000, 10,000, and 2,000 photon histories were processed at $\tau = 0.01$, 1, and 10 respectively.

Flux

The downward diffuse flux at the lower boundary when A = 0 is given in Table I. All flux values are normalized to unit incident flux. When τ is small ($\tau = 0.01$), the flux is also small since there are insufficient water droplets to scatter an appreciable number of photons. The flux increases from each model to the next in the order listed in Table I which corresponds to increasing forward scattering. The Rayleigh model has slightly more forward scattering than the isotropic model and so on down the list. The flux for $\mu_o = -0.1$ would be ten times larger than that for $\mu_o = -1$, if there were no multiple scattering. When $\tau = 0.01$, there is some multiple scattering when $\mu_o = -0.1$ and so the values are somewhat less than ten times the values for $\mu_o = -1$.

When $\tau \blacksquare 1$, the flux at the lower boundary still increases from one model to the next when they are arranged in order of increasing forward scattering. The difference between the isotropic and Rayleigh models on the one hand and the haze and cloud models on the other hand is greater for $\mu_o = -0.1$ than for $\mu_o = -1$.

When $\mu_o = -0.1$, the photon has a greater probability for the isotropic model than for the Rayleigh model of scattering through an angle near 90° that will send it on a vertical downward path. The photon then has a much higher probability of reaching the lower surface when moving in a vertical direction than when its direction cosine is around -0.1, since the optical thickness to the boundary is 10 times larger in the latter case. A somewhat different explanation applies to the haze and cloud models. Here the important factor is the numerous small angle collisions which allow the photon to penetrate much deeper into the medium than they do with the isotropic and Rayleigh models. The photons thus undergo their first large angle scattering from a greater depth in the medium for the haze and cloud models and thus more of them emerge from the lower surface.

The downward diffuse flux reaches a maximum when τ has approximately the value 2 and $\mu_o = -1$. For larger τ values the flux decreases as the photons must undergo more and more collisions to reach the lower boundary. The results for $\tau = 10$ show lower flux values than for $\tau = 1$ for all models except one. The one exception is the nimbostratus model with $\mu_o = -1$; in this case the flux is higher at $\tau = 10$ because of

the extreme forward scattering maximum characteristic of this model. For both angles of incidence at $\tau = 10$, the flux is higher for the isotropic than for the Rayleigh model. The flux increases for the haze and cloud models in the same order as their forward scattering increases. The explanation for these facts is the same as given previously for $\tau = 1$.

Mean Optical Path

The mean optical path for the reflected and transmitted photons is given in Table I. When $\tau = 0.01$ and $\mu_o = -1$, the reflected mean optical path is small for those models that have a relatively high probability for scattering at angles near 180° compared to angles near 90° (Rayleigh, nimbostratus, cumulus); the mean optical path is relatively large when the scattering probability is more nearly equal as these two angles (haze C, haze M, isotropic). For the other τ and μ_o values in Table I, multiple scattering is important. The reflected mean optical path in these cases is always smaller for the isotropic and Rayleigh models than for the haze and cloud models since it is more probable for a photon to change its direction from downward to upward in a specified number of collisions with the former models.

When $\mu_o = -1$, the transmitted mean optical path decreases from one model to the next when they are arranged in order of increasing forward scattering (the only exception at $\tau = 0.01$ between the cumulus and nimbostratus models is either a statistical fluctuation in the results or is connected with details of the forward scattering function). The

photon can obviously traverse the medium in a more nearly vertical direction and thus has a smaller mean optical path as the small angle forward scattering increases. This is particularly striking at $\tau = 10$ where the mean optical paths are 57.3 and 18.1 for the isotropic and nimbostratus models respectively.

When $\mu_o = -0.1$ the above phenomenon is combined with the probability of the photon making a large angle collision that sends it in approximately a downward vertical direction. When $\tau = 0.01$ the photon travels farther along the original direction for the haze and cloud models as compared to the isotropic and Rayleigh models before on the average undergoing a large angle scattering and thus the reflected mean optical paths are larger for the former models. For $\tau \blacksquare 10$, the results are just the opposite. The most important factor in this case is that the photon after making a large angle collision so that it is travelling almost vertically downward can then move more easily toward the lower boundary when aided by numerous small angle collisions.

Cloud Albedo

The cloud albedo when $A = 0$ is also given in Table I. For a given optical thickness and angle of incidence, the cloud albedo decreases in value from one model to the next when they are arranged in order of increasing forward scattering. The only exceptions to this statement occur in the comparison between the isotropic and Rayleigh models due to either the very small difference between the scattering function for these models when averged over the appropriate angle or to

fluctuations in the Monte Carlo results. The differences in the cloud albedo between the other models are very striking. When there is greater forward scattering, the photon penetrates to a deeper layer before undergoing a collision which sends it in an upward direction. The result is fewer photons escaping from the upper surface of the cloud and a lower cloud albedo.

Angular Half-width of Downward Diffuse Radiation

The scattering functions for the cumulus and nimbostratus models have very strong maxima in the forward direction (as do the haze C and haze M models to a lesser extent). The result is that the diffuse radiation has a sharp maximum around the incident direction until quite large optical depths are reached. Although our graphs for the transmitted intensity averaged over a μ interval of 0.1 often show a maximum in the direction of the incident beam, the remarkable sharpness of this maximum is hidden by the averaging process.

In order to investigate the angular spread of the diffuse radiation as a function of optical depth, calculations were made for the nimbostratus model with extremely fine angular intervals. The results are shown in Figures 16 and 17. The downward diffuse radiance was calculated for $\tau = 10$, $\mu_o = -1$, and $A = 0$. The downward radiance in the various angular intervals was recorded by eight detectors located at $\tau = 0.1$, 0.3, 1, 2, 3, 5, 8, and 10. In order to show the relative spread in the radiance, all the values have been normalized to unity at $\mu = -1$. There is somewhat more fluctuation in the values very

close to $\mu = -1$ than in the remaining values. When $\mu_o = -0.99995$ (an angle of 0°35' with the vertical) the radiance has fallen to less than half its value at $\mu_o = -1$ for all detectors with $\tau \leq 3$. The radiance at the detector at $\tau = 0.1$ is 0.1 or 0.001 of its value in the incident direction at an angle of approximately 1° or 5° with the vertical respectively. Even at the large optical thickness $\tau = 10$, the radiance is 0.5 of its value in the incident direction at an angle of approximately 1°20' with the vertical; the variation of the radiance with angle is still controlled by the numerous small angle scattering events at $\tau = 10$.

At all optical depths shown in Figures 16 and 17 the radiance has a very strong sharp maximum around the initial beam direction. This illustrates once again the importance of including an accurate treatment of the numerous small angle scattering events in any theoretical calculations of multiple scattering.

Table I.

Mean Optical Path, Flux at Lower Boundary for A=0, and Cloud Albedo for A=0

Model	τ	μ_o	Reflected mean optical path	Transmitted mean optical path	Diffuse flux at lower boundary	Cloud albedo
Isotropic	0.01	-0.1	0.0938	0.0962	0.0476	0.0476
Rayleigh	0.01	-0.1	0.0966	0.100	0.0481	0.0470
Haze C	0.01	-0.1	0.157	0.129	0.0584	0.0367
Haze M	0.01	-0.1	0.179	0.140	0.0617	0.0334
Cumulus	0.01	-0.1	0.194	0.123	0.0734	0.0218
Nimbostratus	0.01	-0.1	0.204	0.124	0.0745	0.0207
Isotropic	1	-0.1	2.66	3.73	0.306	0.694
Rayleigh	1	-0.1	2.63	3.80	0.292	0.708
Haze C	1	-0.1	3.68	4.86	0.414	0.586
Haze M	1	-0.1	4.10	5.27	0.438	0.561
Cumulus	1	-0.1	4.89	6.34	0.466	0.534
Nimbostratus	1	-0.1	5.23	6.48	0.482	0.518
Isotropic	10	-0.1	9.77	55.0	0.0697	0.930
Rayleigh	10	-0.1	9.26	52.9	0.0607	0.939
Haze C	10	-0.1	11.0	28.8	0.151	0.849
Haze M	10	-0.1	11.6	27.8	0.176	0.824
Cumulus	10	-0.1	12.9	28.0	0.201	0.799
Nimbostratus	10	-0.1	13.7	27.6	0.239	0.761
Isotropic	0.01	-1	0.0534	0.0484	0.00493	0.00502
Rayleigh	0.01	-1	0.0412	0.0468	0.00497	0.00498
Haze C	0.01	-1	0.0660	0.0160	0.00927	0.000678
Haze M	0.01	-1	0.0651	0.0137	0.00940	0.000545
Cumulus	0.01	-1	0.0405	0.0116	0.00950	0.000445
Nimbostratus	0.01	-1	0.0398	0.0122	0.00962	0.000332
Isotropic	1	-1	2.58	2.82	0.285	0.347
Rayleigh	1	-1	2.50	2.73	0.289	0.343
Haze C	1	-1	4.12	1.48	0.553	0.0794
Haze M	1	-1	4.14	1.34	0.569	0.0628
Cumulus	1	-1	3.75	1.23	0.583	0.0487
Nimbostratus	1	-1	3.80	1.17	0.595	0.0372
Isotropic	10	-1	21.5	57.3	0.158	0.842
Rayleigh	10	-1	21.1	55.2	0.151	0.849
Haze C	10	-1	24.3	23.9	0.435	0.564
Haze M	10	-1	25.4	22.2	0.517	0.483
Cumulus	10	-1	24.2	19.2	0.534	0.466
Nimbostratus	10	-1	26.6	18.1	0.636	0.364

References

1. G. N. Plass and G. W. Kattawar, J. Geoph. Res. (in press).

2. S. Fritz, J. Meteor. 11, 291 (1954).

3. S. Fritz, J. Opt. Soc. Amer. 10, 820 (1955).

4. S. Twomey, H. Jacobowitz, and H. B. Howell, J. Atm. Sci. 24, 70 (1967).

5. J. M. Hammersley and D. C. Handscomb, Monte Carlo Methods (John Wiley and Sons, Inc., New York, 1964).

6. D. G. Collins and M. B. Wells, Monte Carlo Codes for the Study of Light Transport in the Atmosphere, Vols, I and II, Radiation Research Associates, Inc., Fort Worth, Texas, 1965.

7. D. Deirmendjian, Appl. Opt, 3, 187 (1964).

8. M. Dien, Met. Rundschau 1, 261 (1948).

9. L. W. Carrier, G. A. Cato, K. J. von Essen, Appl. Opt. 6, 1209 (1967).

10. G. W. Kattawar, G. N. Plass Appl. Opt. 6, 1377 (1967).

Captions for Figures

Fig. 1. Angular scattering function for Mie scattering as a function of the cosine of scattering angle Θ averaged over the size distributions given by Eqs. (1-4) and for isotropic and Rayleigh scattering. The curves are averaged over the two directions of polarization. The inset in the upper left shows the curves near $\mu = 1$ and in the upper right near $\mu = -1$. The wavelength of the incident light is 0.7μ and the index of refraction of the water droplets is 1.33.

Fig. 2. Reflected radiance as a function of μ, the cosine of the zenith angle for various particle distributions. The curves on the left and right portion of the figure are for A (surface albedo) = 0 and 1 respectively. The optical depth of the cloud $\tau = 0.01$. The sunlight is incident vertically, μ_o (cosine of incident zenith angle) = -1.0. The single scattering albedo is unity. The incident flux is normalized to unity. The squares indicate the radiance for single scattering only calculated directly from the scattering function.

Fig. 3. Reflected radiance for $\tau = 1$ and $\mu_o = -1$ as a function of μ. See caption for Fig. 2.

Fig. 4. Reflected radiance for $\tau = 10$ and $\mu_o = -1$ as a function of μ. See caption for Fig. 2.

Fig. 5. Reflected radiance for $\tau = 0.01$, $\mu_o = -0.1$, and A = 0 as a function of μ. The left hand portion of the graph refers to values averaged over the azimuthal angle for 90° on both sides of the original beam. The values on the right portion of the

graph are for values averaged over the remaining azimuthal angles. Thus one intensity curve from left to right shows the variation from one horizon to the zenith and back to the other horizon averaged over the indicated azimuthal angles.

Fig. 6. Reflected radiance for $\tau = 1$, $\mu_o = -0.1$, and $A = 0$ as a function of μ. See caption for Fig. 5.

Fig. 7. Reflected radiance for $\tau = 1$, $\mu_o = -0.1$, and $A = 1$ as a function of μ. See caption for Fig. 5.

Fig. 8. Reflected radiance for $\tau = 10$, $\mu_o = -0.1$, and $A = 0$ as a function of μ. See caption for Fig. 5.

Fig. 9. Transmitted radiance for $\tau = 0.01$ and $\mu_o = -1$ as a function of μ. This is the diffuse radiance without the original beam. See caption for Fig. 2.

Fig. 10. Transmitted radiance for $\tau = 1$ and $\mu_o = -1$ as a function of μ. See caption for Fig. 2.

Fig. 11. Transmitted radiance for $\tau = 10$ and $\mu_o = -1$ as a function of μ. See caption for Fig. 2.

Fig. 12. Transmitted radiance for $\tau = 0.01$, $\mu_o = -0.1$, and $A = 0$ as a function of μ. See caption for Fig. 5.

Fig. 13 Transmitted radiance for $\tau = 1$, $\mu_o = -0.1$, and $A = 0$ as a function of μ. See caption for Fig. 5.

Fig. 14. Transmitted radiance for $\tau = 1$, $\mu_o = -0.1$, and $A = 1$ as a function of μ. See caption for Fig. 5.

Fig. 15. Transmitted radiance for $\tau = 10$, $\mu_o = -0.1$, and $A = 0$ as a function of μ. See caption for Fig. 5.

Fig. 16. Downward diffuse radiance for nimbostratus model for $\tau = 10$, $\mu_o = -1$, and $A = 0$. The values of the radiance at detectors at various levels in the cloud are shown as a function of μ. Only values very close to the incident direction are shown in this figure. The radiance at each level is normalized to unity in the vertical direction in order to show the relative variation at each detector. See Fig. 17.

Fig. 17. Same as Fig. 16 except showing a different range of μ values. The first μ interval shown here is the next interval following the last μ interval in Fig. 16. The intervals shown in Fig. 16 cannot be shown here because of the scale. The radiance at each level is normalized to unity in the vertical direction.

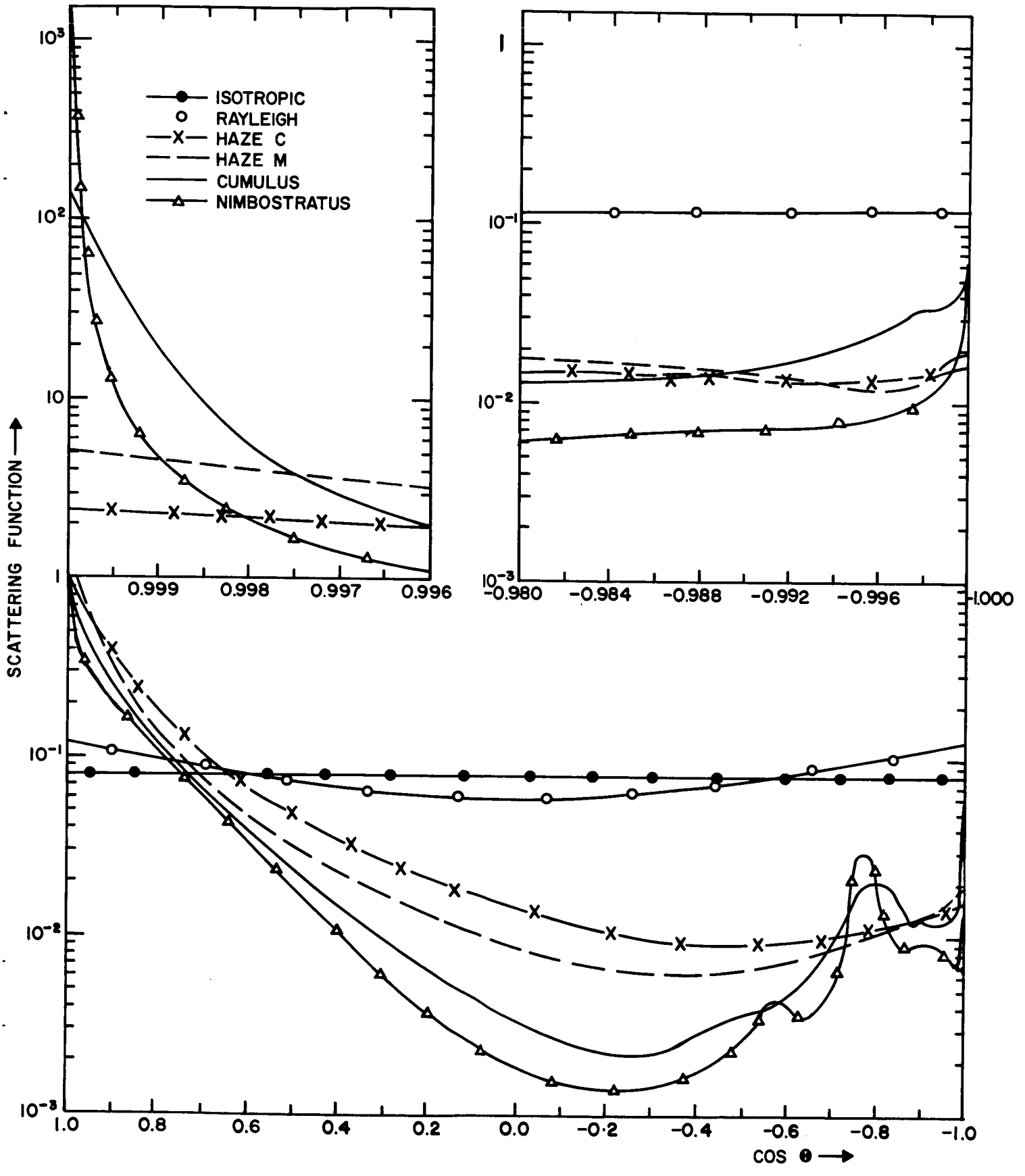
ISOTROPIC
RAYLEIGH
HAZE C
HAZE M
CUMULUS
NIMBOSTRATUS
SCATTERING FUNCTION
COS θ
10³
10²
10
1
10⁻¹
10⁻²
10⁻³
1.0
0.8
0.6
0.4
0.2
0.0
-0.2
-0.4
-0.6
-0.8
-1.0
0.999
0.998
0.997
0.996
-0.980
-0.984
-0.988
-0.992
-0.996
-1.000

FIGURE 1

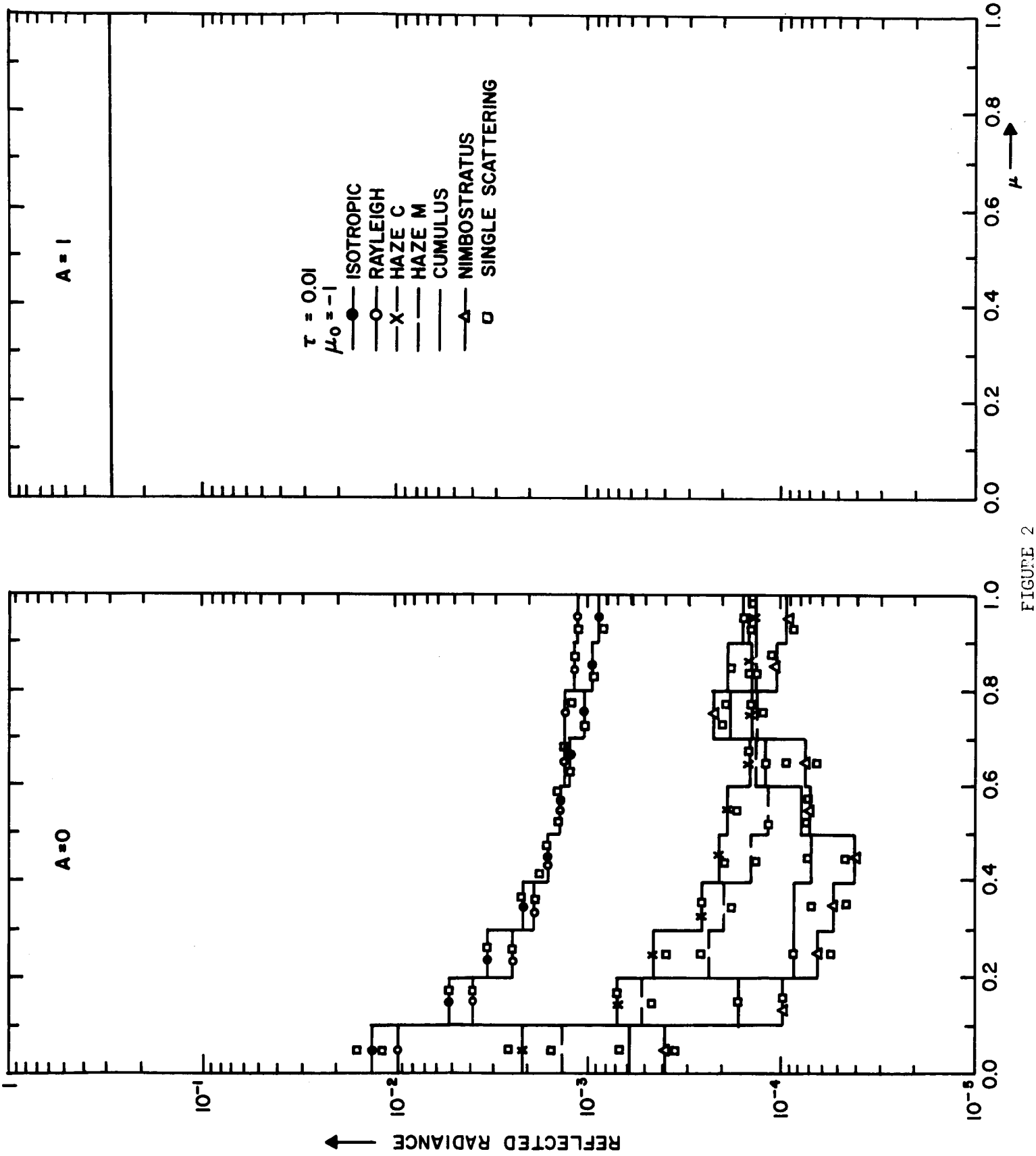
A = 1
τ = 0.01
μ0 = -1
ISOTROPIC
RAYLEIGH
HAZE C
HAZE M
CUMULUS
NIMBOSTRATUS
SINGLE SCATTERING
0.0
0.2
0.4
0.6
0.8
1.0
μ
A=0
1
10-1
10-2
10-3
10-4
10-5
REFLECTED RADIANCE

FIGURE 2

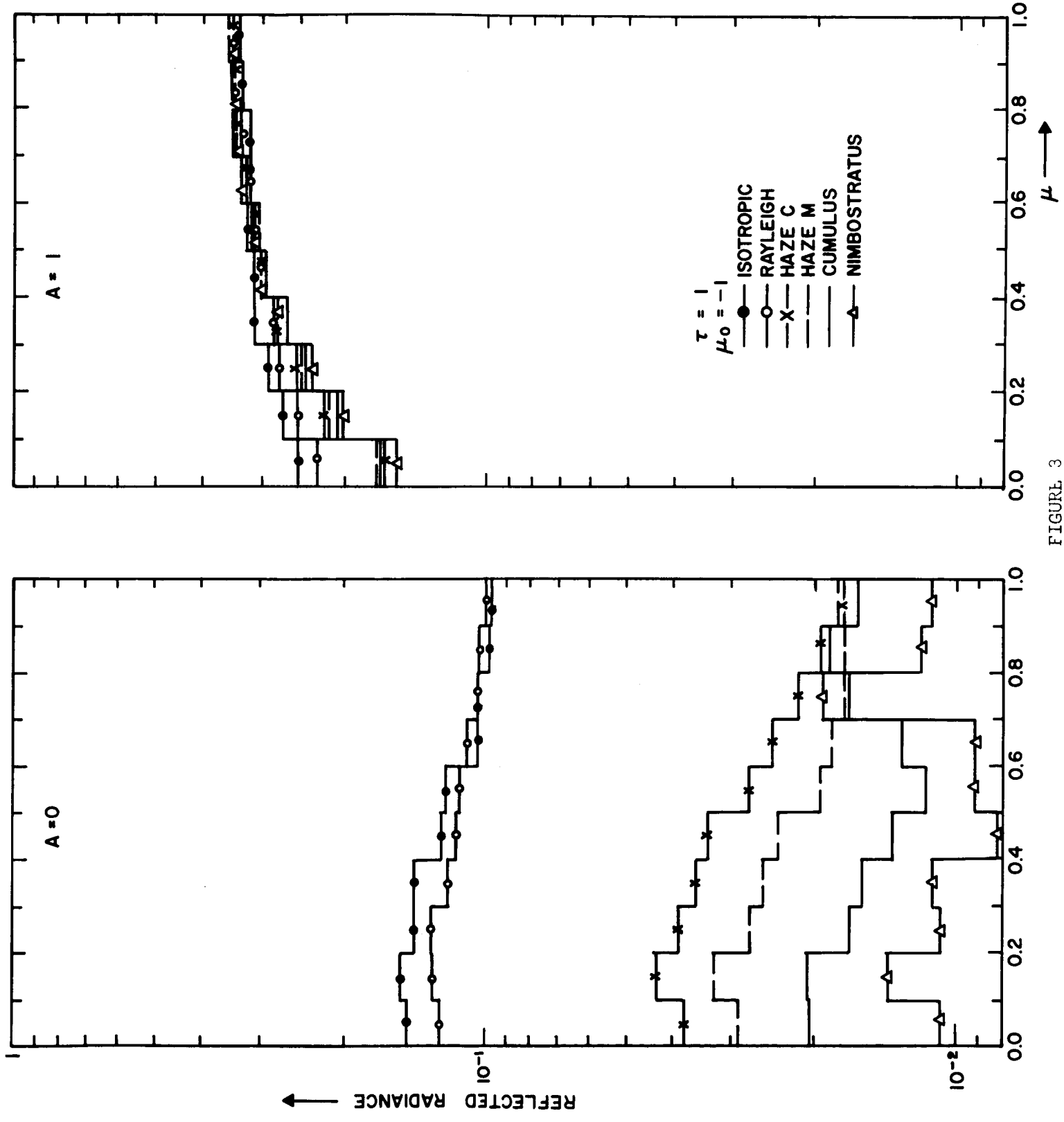
A = 1
A = 0
τ = 1
μ0 = −1
ISOTROPIC
RAYLEIGH
HAZE C
HAZE M
CUMULUS
NIMBOSTRATUS
μ
REFLECTED RADIANCE
10⁻¹
10⁻²
0.0
0.2
0.4
0.6
0.8
1.0

FIGURE 3

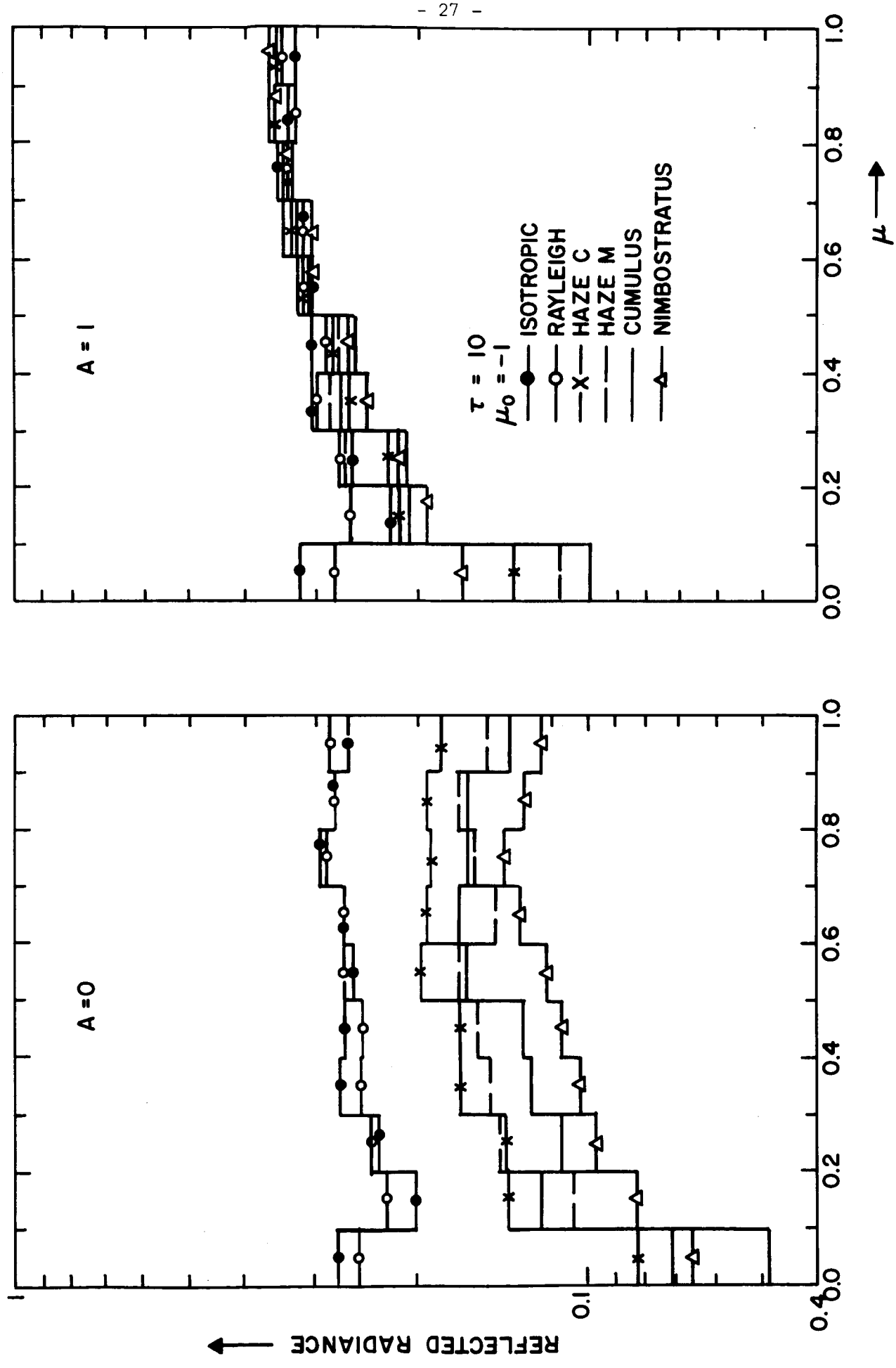
A = 1
τ = 10
μ0 = -1
ISOTROPIC
RAYLEIGH
HAZE C
HAZE M
CUMULUS
NIMBOSTRATUS
μ
A = 0
REFLECTED RADIANCE
0.0
0.2
0.4
0.6
0.8
1.0
0.1

FIGURE 4

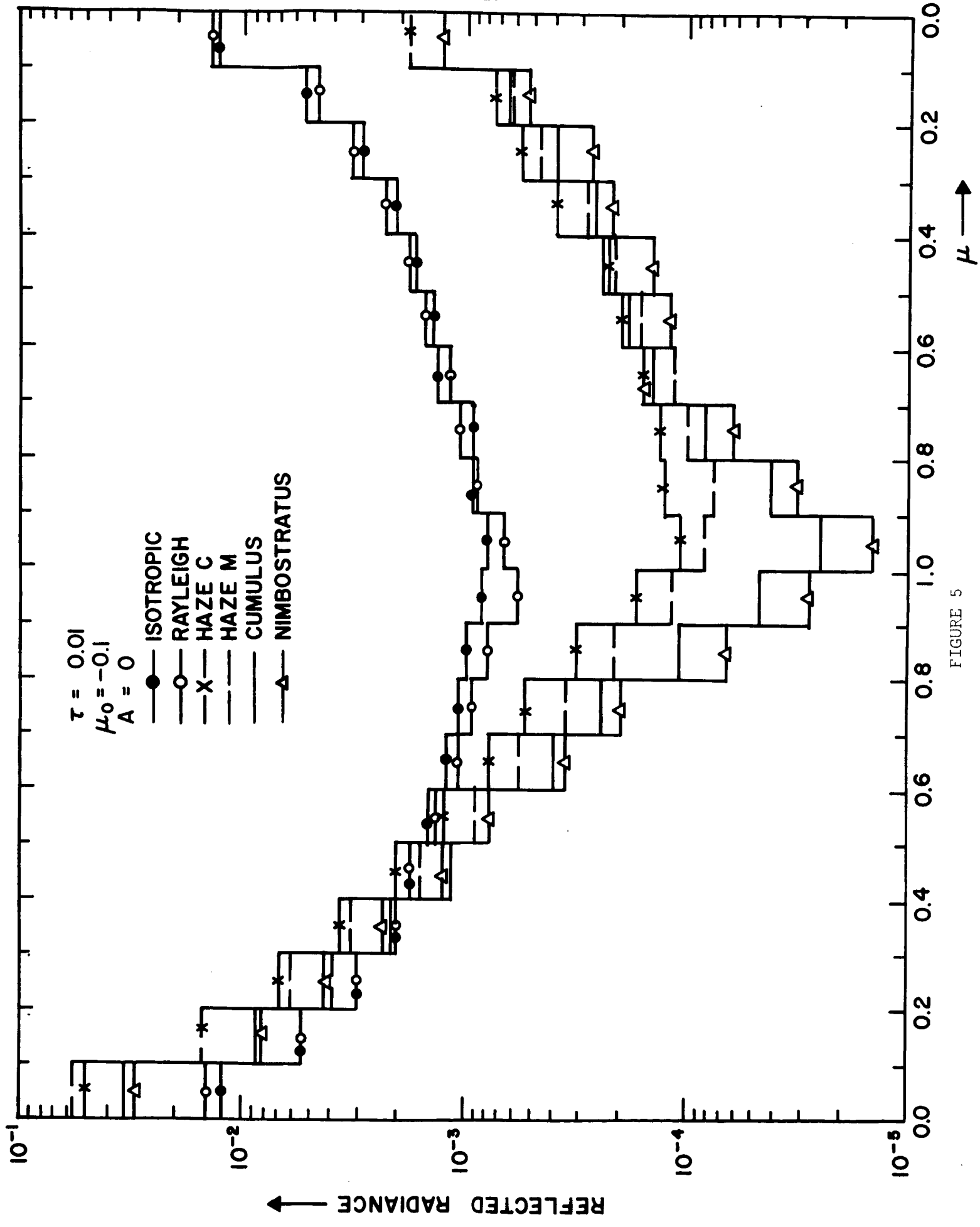
τ = 0.01
μ0 = −0.1
A = 0
ISOTROPIC
RAYLEIGH
HAZE C
HAZE M
CUMULUS
NIMBOSTRATUS
REFLECTED RADIANCE
10−1
10−2
10−3
10−4
10−5
0.0
0.2
0.4
0.6
0.8
1.0
μ

FIGURE 5

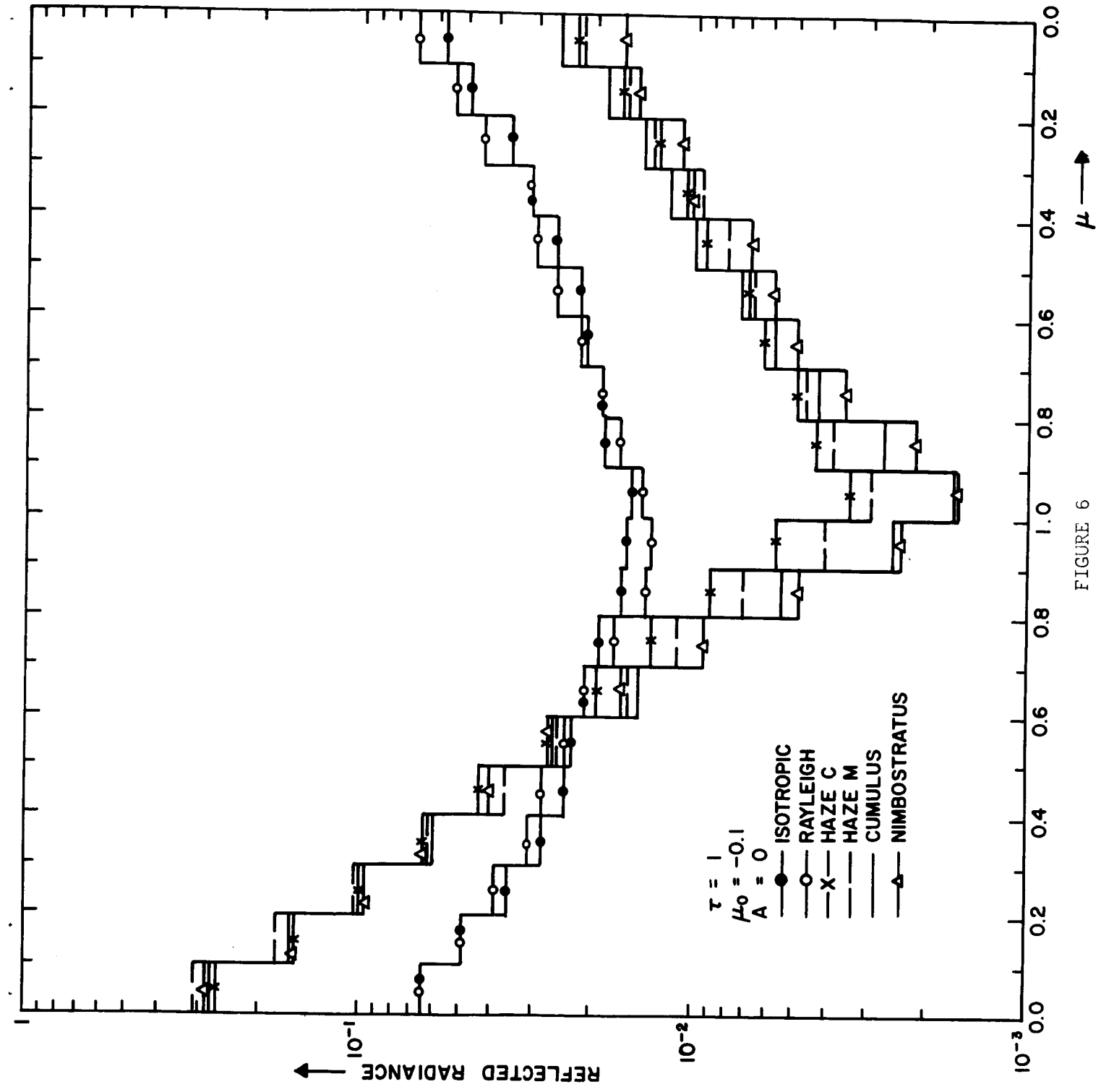
REFLECTED RADIANCE
10^{-1}
10^{-2}
10^{-3}
0.0
0.2
0.4
0.6
0.8
1.0
μ
τ = 1
μ_0 = -0.1
A = 0
ISOTROPIC
RAYLEIGH
HAZE C
HAZE M
CUMULUS
NIMBOSTRATUS

FIGURE 6

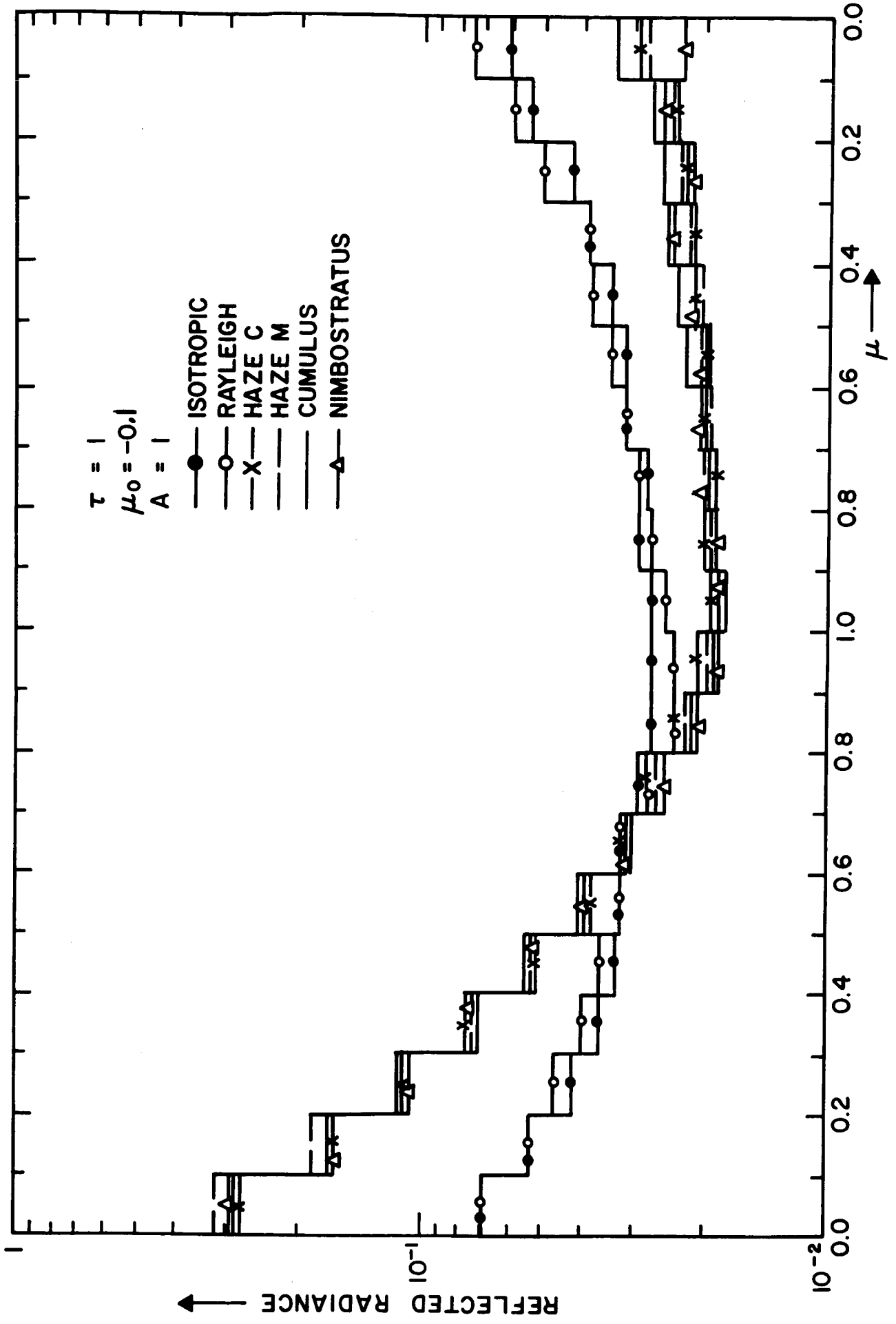
τ = 1
μ0 = -0.1
A = 1
ISOTROPIC
RAYLEIGH
HAZE C
HAZE M
CUMULUS
NIMBOSTRATUS
REFLECTED RADIANCE
1
10-1
10-2
0.0
0.2
0.4
0.6
0.8
1.0
μ

FIGURE 7

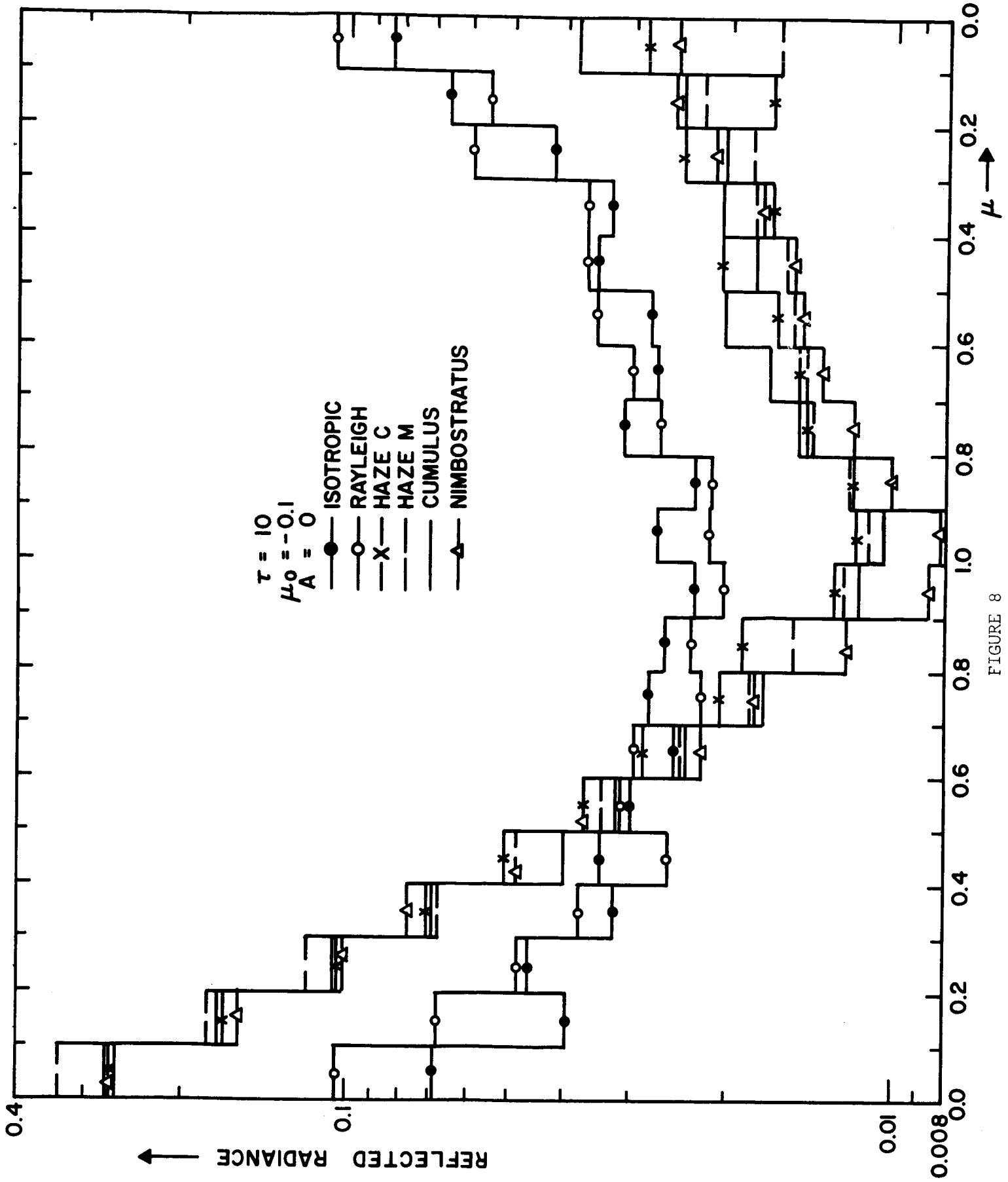
τ = 10
μ0 = -0.1
A = 0
ISOTROPIC
RAYLEIGH
HAZE C
HAZE M
CUMULUS
NIMBOSTRATUS
REFLECTED RADIANCE
0.4
0.1
0.01
0.008
0.0
0.2
0.4
0.6
0.8
1.0
0.8
0.6
0.4
0.2
0.0
μ

FIGURE 8

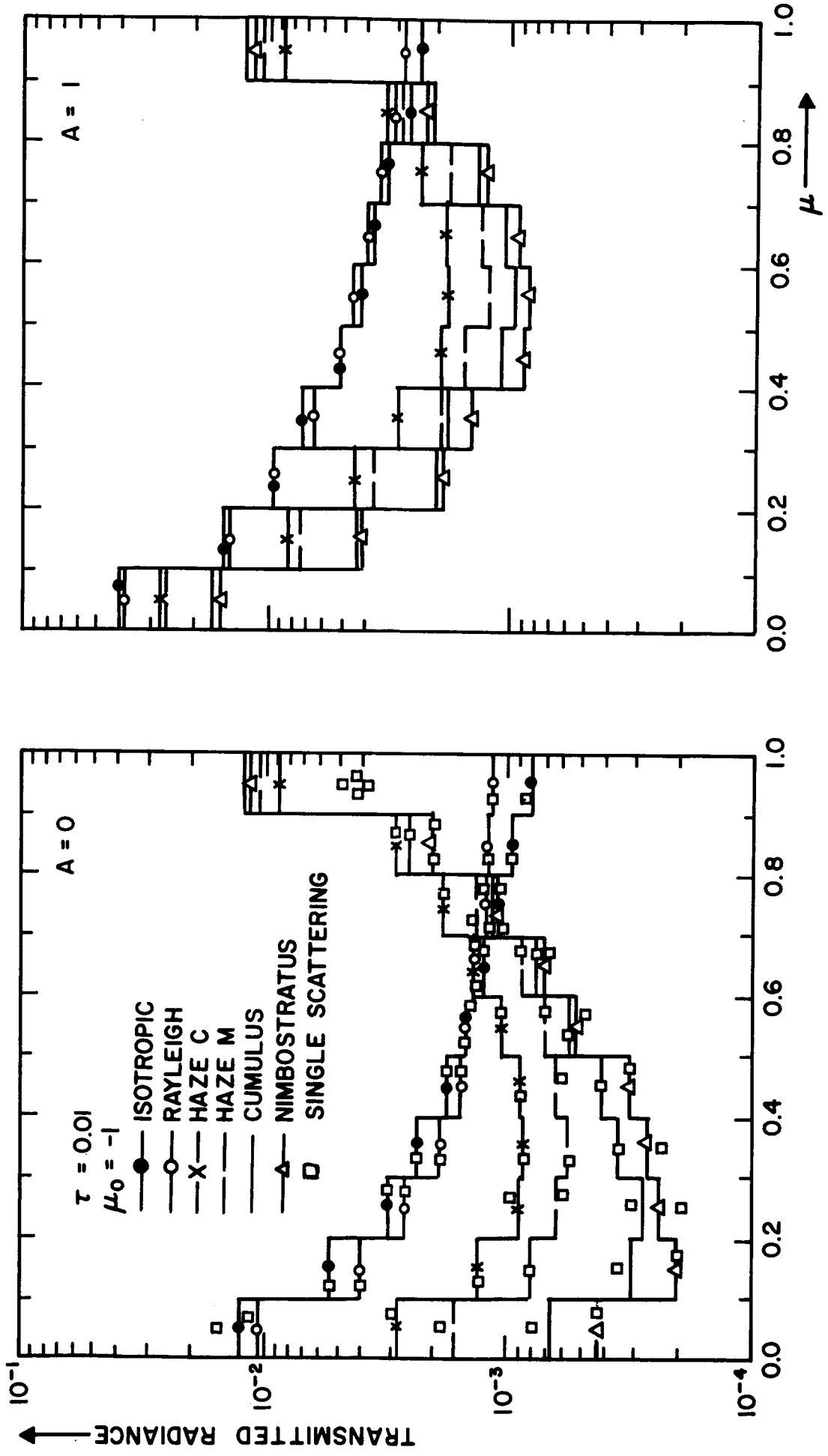
A = 0
τ = 0.01
μ0 = -1
ISOTROPIC
RAYLEIGH
HAZE C
HAZE M
CUMULUS
NIMBOSTRATUS
SINGLE SCATTERING
TRANSMITTED RADIANCE
10^-1
10^-2
10^-3
10^-4
0.0
0.2
0.4
0.6
0.8
1.0
A = 1
μ

FIGURE 9

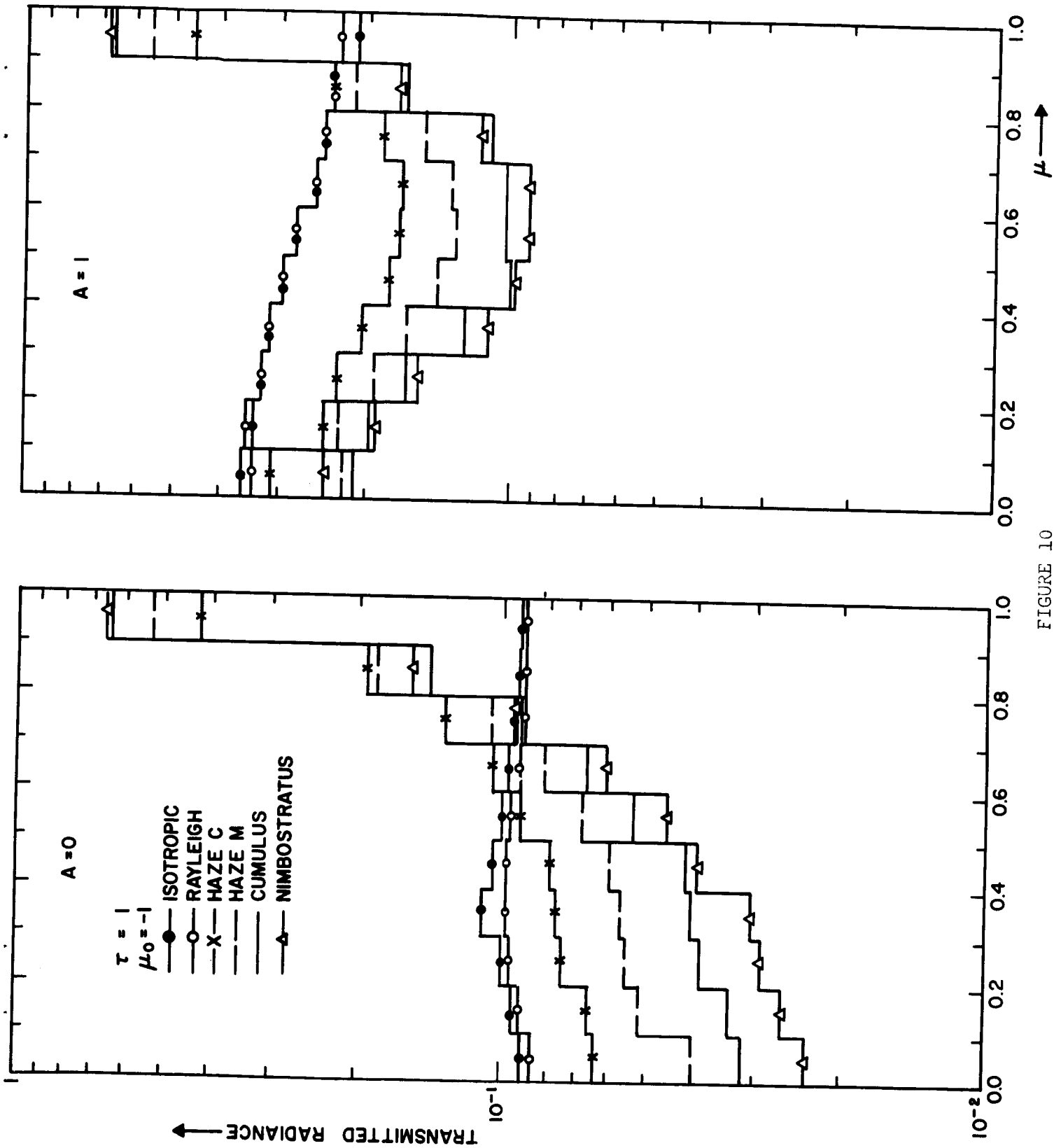
A = 1
A = 0
τ = 1
μ0 = -1
ISOTROPIC
RAYLEIGH
HAZE C
HAZE M
CUMULUS
NIMBOSTRATUS
TRANSMITTED RADIANCE
μ
1.0
0.8
0.6
0.4
0.2
0.0
10⁻¹
10⁻²

FIGURE 10

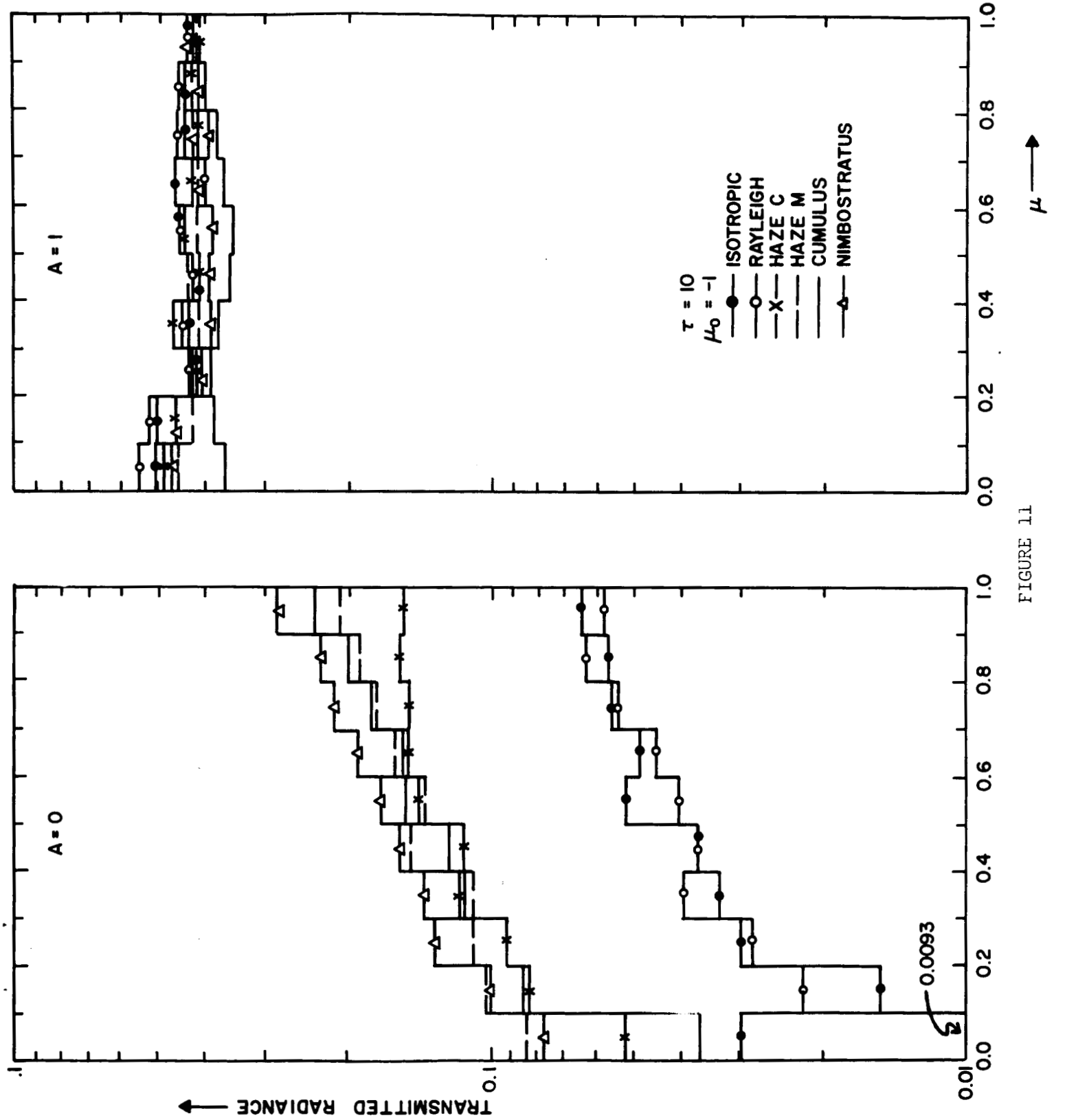
A = 0
A = 1
τ = 10
μ0 = -1
ISOTROPIC
RAYLEIGH
HAZE C
HAZE M
CUMULUS
NIMBOSTRATUS
0.0093
TRANSMITTED RADIANCE
μ
0.0
0.2
0.4
0.6
0.8
1.0
0.01
0.1
1.0

FIGURE 11

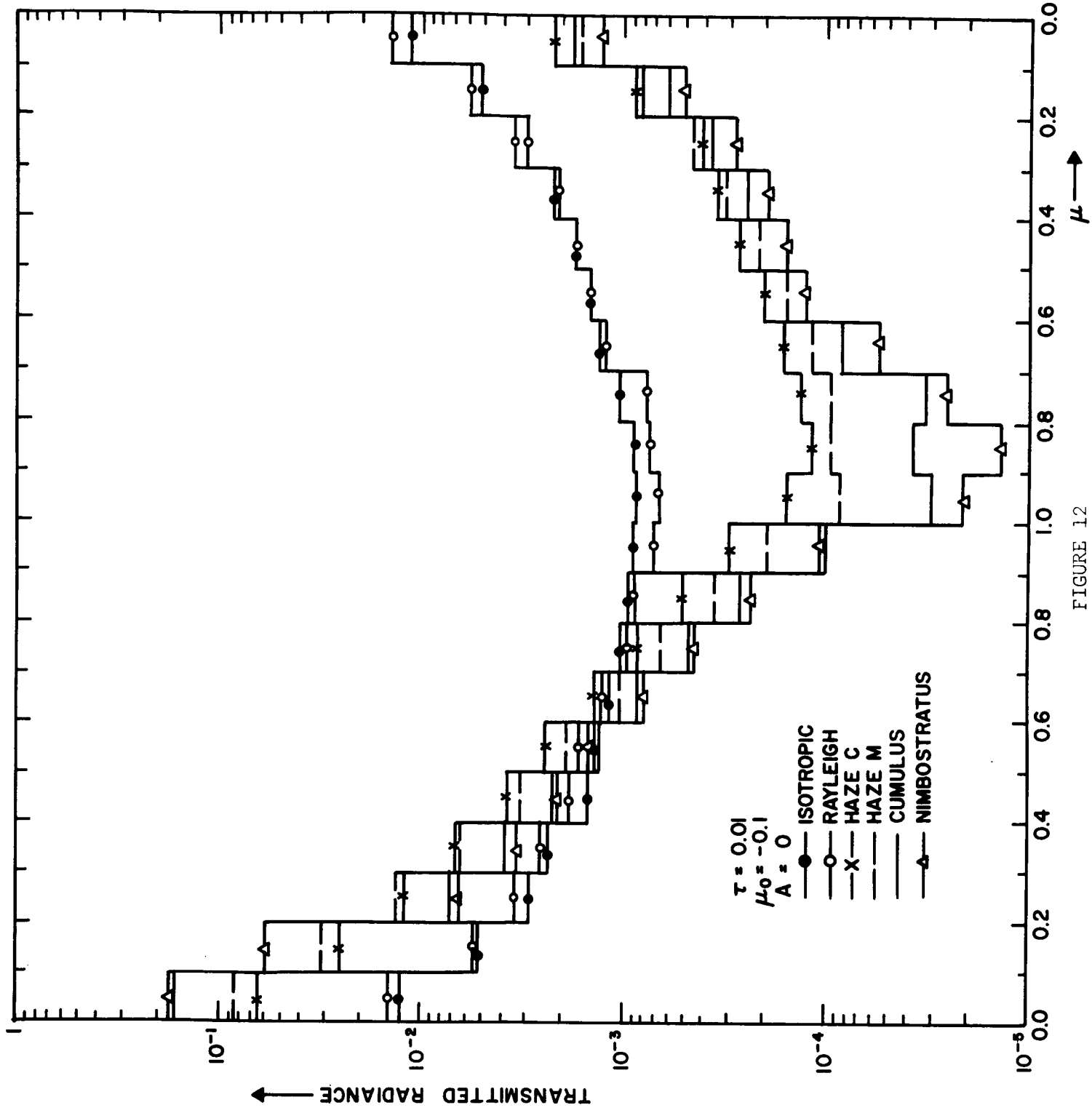
TRANSMITTED RADIANCE
1
10^{-1}
10^{-2}
10^{-3}
10^{-4}
10^{-5}
0.0
0.2
0.4
0.6
0.8
1.0
μ
τ = 0.01
μ_0 = -0.1
A = 0
ISOTROPIC
RAYLEIGH
HAZE C
HAZE M
CUMULUS
NIMBOSTRATUS

FIGURE 12

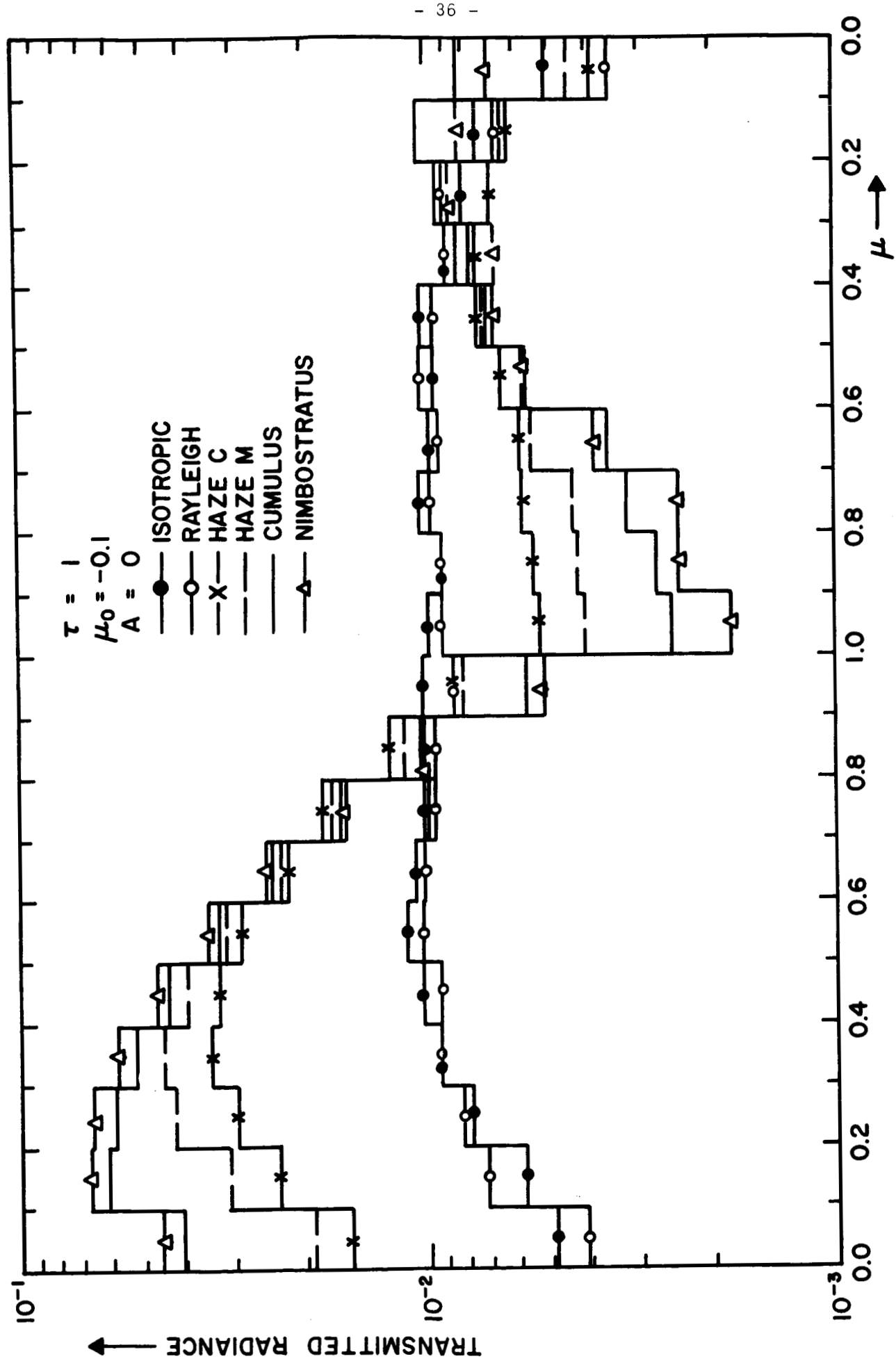
τ = 1
μ0 = -0.1
A = 0
ISOTROPIC
RAYLEIGH
HAZE C
HAZE M
CUMULUS
NIMBOSTRATUS
TRANSMITTED RADIANCE
10-1
10-2
10-3
0.0
0.2
0.4
0.6
0.8
1.0
μ

FIGURE 13

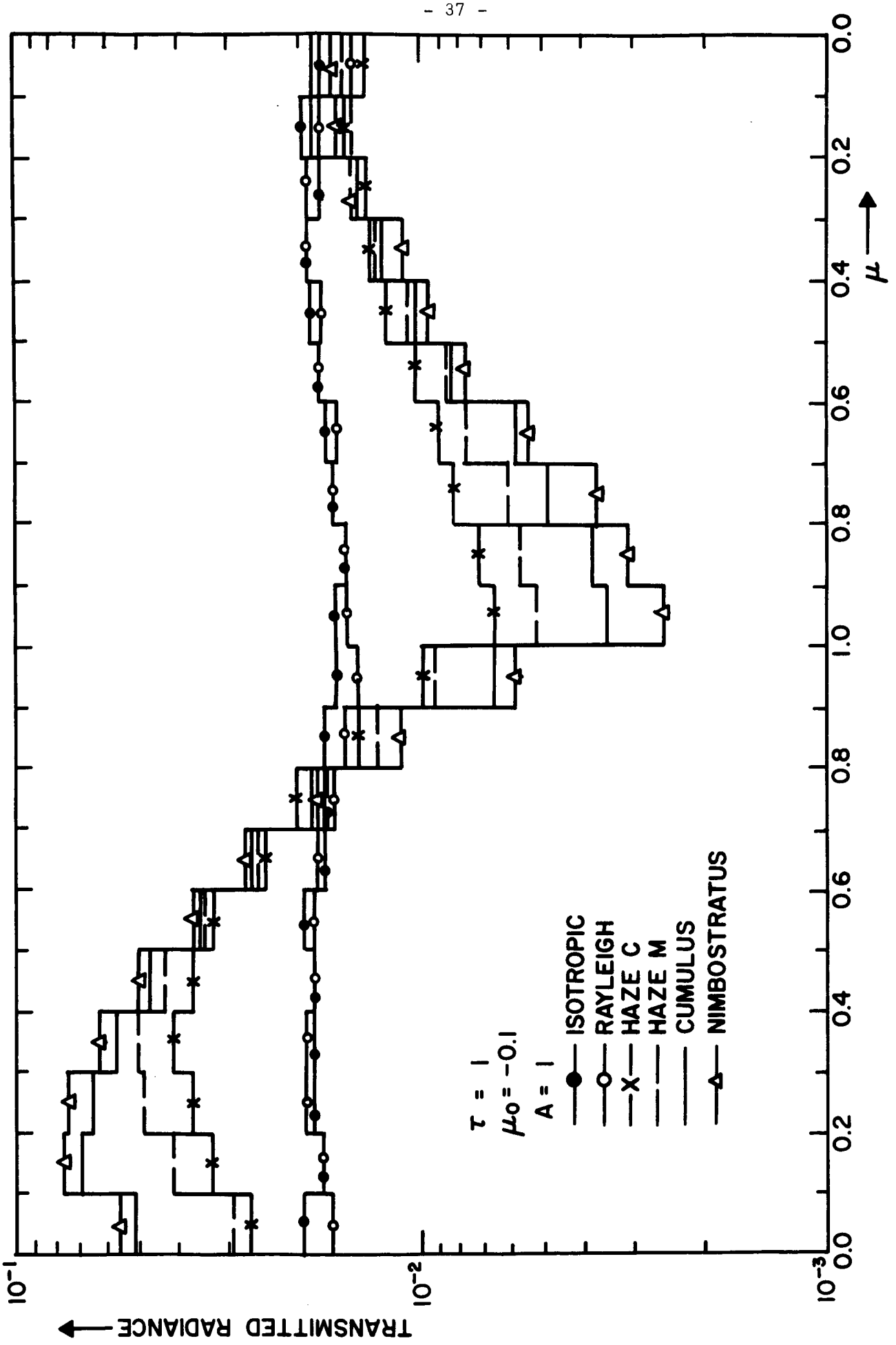
TRANSMITTED RADIANCE
10^{-1}
10^{-2}
10^{-3}
0.0
0.2
0.4
0.6
0.8
1.0
0.8
0.6
0.4
0.2
0.0
μ
$\tau = 1$
$\mu_0 = -0.1$
$A = 1$
ISOTROPIC
RAYLEIGH
HAZE C
HAZE M
CUMULUS
NIMBOSTRATUS

FIGURE 14

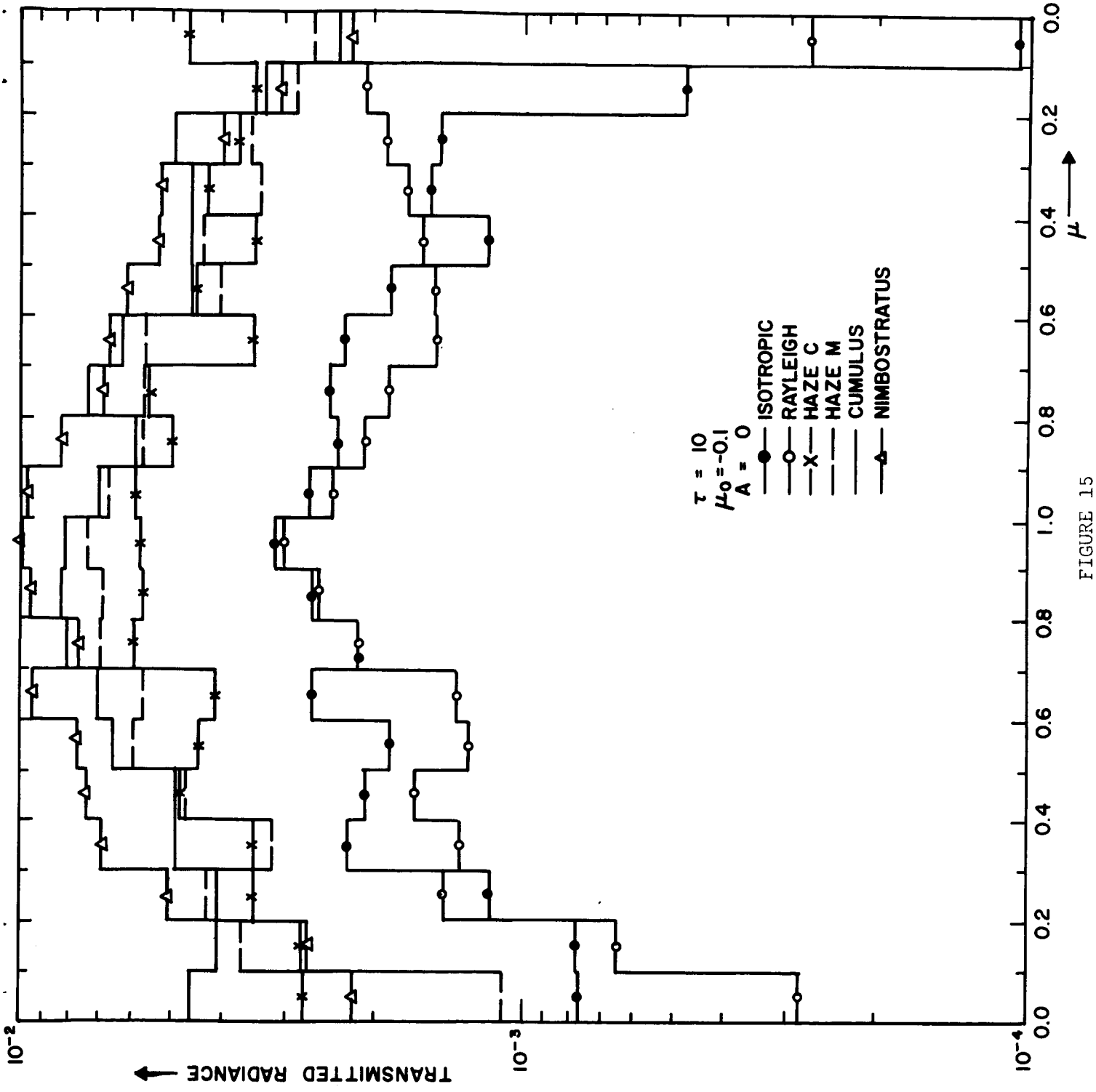
TRANSMITTED RADIANCE
10^{-2}
10^{-3}
10^{-4}
0.0
0.2
0.4
0.6
0.8
1.0
μ
τ = 10
μ_0 = -0.1
A = 0
ISOTROPIC
RAYLEIGH
HAZE C
HAZE M
CUMULUS
NIMBOSTRATUS

FIGURE 15

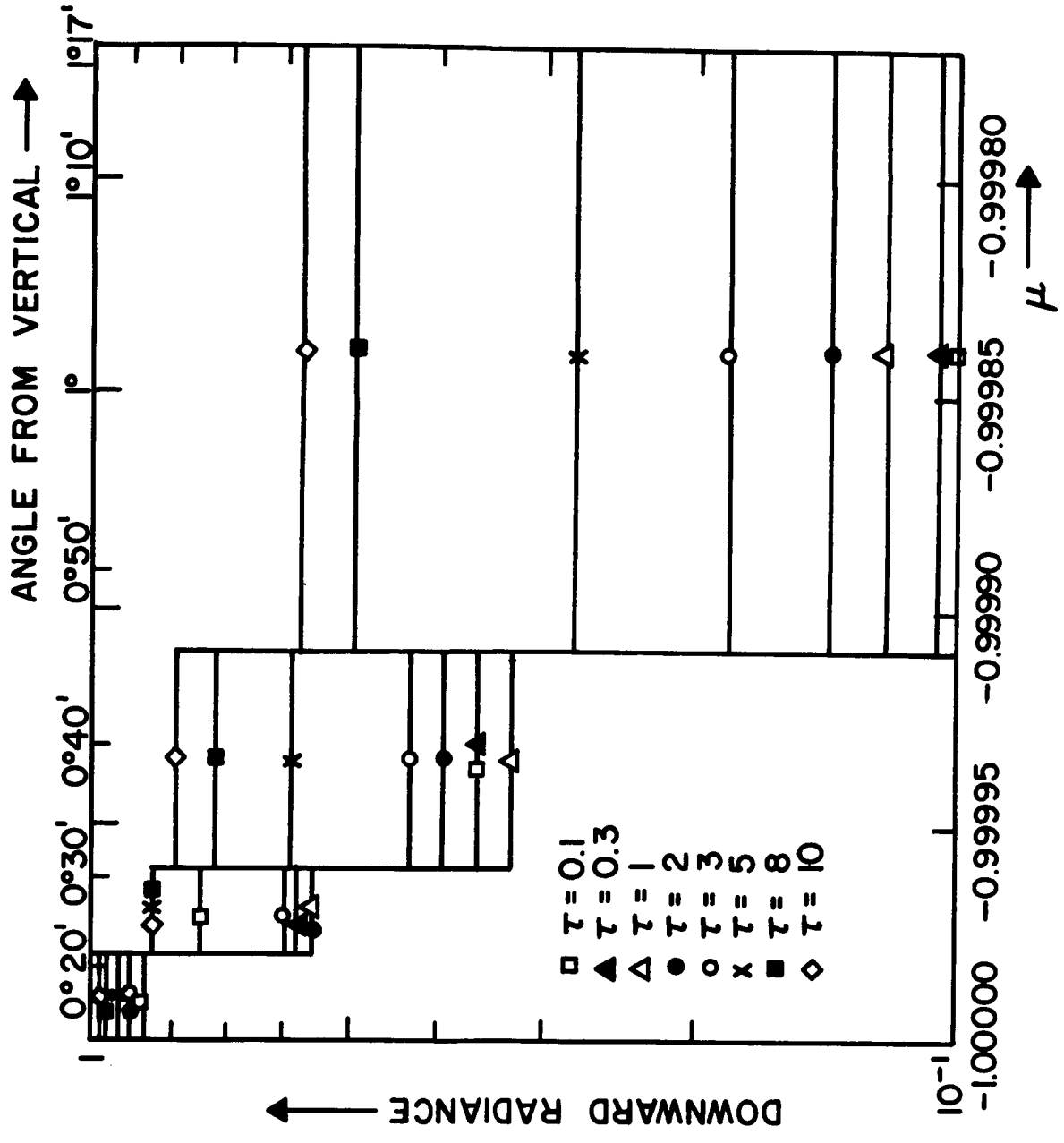
ANGLE FROM VERTICAL
0°20'
0°30'
0°40'
0°50'
1°
1°10'
1°17'
DOWNWARD RADIANCE
1
10⁻¹
10⁻²
μ
0.99995
0.99990
0.99985
0.99980
τ = 0.1
τ = 0.3
τ = 1
τ = 2
τ = 3
τ = 5
τ = 8
τ = 10

FIGURE 16

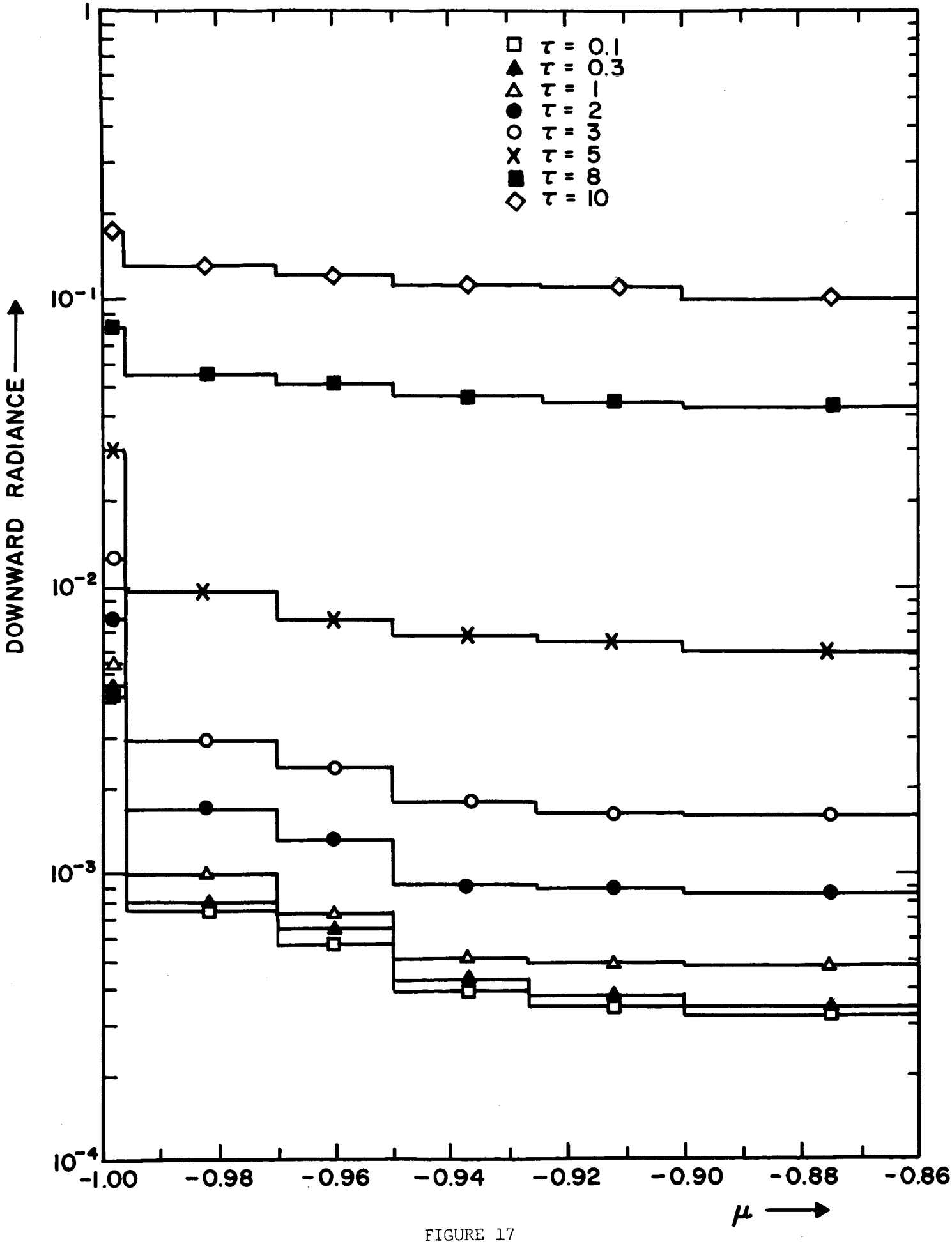
τ = 0.1
τ = 0.3
τ = 1
τ = 2
τ = 3
τ = 5
τ = 8
τ = 10
DOWNWARD RADIANCE
1
10⁻¹
10⁻²
10⁻³
10⁻⁴
-1.00
-0.98
-0.96
-0.94
-0.92
-0.90
-0.88
-0.86
μ

FIGURE 17

Unclassified
Security Classification

DOCUMENT CONTROL DATA - R & D

(Security classification of title, body of abstract and indexing annotation must be entered when the overall report is classified)

1. ORIGINATING ACTIVITY (Corporate author)	2a. REPORT SECURITY CLASSIFICATION
Southwest Center for Advanced Studies Dallas, Texas 75230	Unclassified
	2b. GROUP

3. REPORT TITLE

INFLUENCE OF PARTICLE SIZE DISTRIBUTION ON REFLECTED AND TRANSMITTED LIGHT FROM CLOUDS

4. DESCRIPTIVE NOTES *(Type of report and inclusive dates)*

Scientific. Interim.

5. AUTHOR(S) *(First name, middle initial, last name)*

George W. Kattawar
Gilbert N. Plass

6. REPORT DATE	7a. TOTAL NO. OF PAGES	7b. NO. OF REFS
24 August 1967	41	10

8a. CONTRACT OR GRANT NO.	9a. ORIGINATOR'S REPORT NUMBER(S)
AF19(628)-5039 b. PROJECT NO. 4076- 04 c. 62405484 634076	Scientific Report No. 5 9b. OTHER REPORT NO(S) *(Any other numbers that may be assigned this report)* AFCRL-

10. DISTRIBUTION STATEMENT

Distribution of this document is unlimited. It may be released to the Clearinghouse, Department of Commerce, for sale to the general public.

11. SUPPLEMENTARY NOTES	12. SPONSORING MILITARY ACTIVITY
also by the National Aeronautics and Space Administration contract	Air Force Cambridge Research Laboratories (CRO), L. G. Hanscom Field Bedford, Massachusetts 01730

13. ABSTRACT

The light reflected and transmitted from clouds with various drop size distributions is calculated by a Monte Carlo technique. Six different models are used for the drop size distribution: isotropic; Rayleigh; haze continental; haze maritime; cumulus; nimbostratus. The scattering function for each model is calculated from the Mie theory. In general the reflected and transmitted radiance for the isotropic and Rayleigh models tend to be similar as are those for the various haze and cloud models. The reflected radiance is less for the haze and cloud models than for the isotropic and Rayleigh models, except for an angle of incidence near the horizon when it is larger around the incident beam direction. The transmitted radiance is always much larger for the haze and cloud models near the incident direction; at distant angles it is less for small and moderate optical thicknesses and greater for large optical thicknesses (all comparisons to isotropic and Rayleigh models). The downward flux, cloud albedo, and mean optical path are discussed. The angular spread of the beam as a function of optical thickness is shown for the nimbostratus model.

DD FORM 1 NOV 65 1473

Unclassified
Security Classification

14 KEY WORDS	LINK A		LINK B		LINK C	
	ROLE	WT	ROLE	WT	ROLE	WT
Reflected radiance						
Transmitted radiance						
Clouds						
Particle size distribution						

Unclassified
Security Classification

DOCUMENT CONTROL DATA - R & D

(Security classification of title, body of abstract and indexing annotation must be entered when the overall report is classified)

1. ORIGINATING ACTIVITY (Corporate author)	2a. REPORT SECURITY CLASSIFICATION
Southwest Center for Advanced Studies Dallas, Texas 75230	Unclassified
	2b. GROUP

3. REPORT TITLE

INFLUENCE OF PARTICLE SIZE DISTRIBUTION ON REFLECTED AND TRANSMITTED LIGHT FROM CLOUDS

4. DESCRIPTIVE NOTES (Type of report and inclusive dates)

Scientific. Interim.

5. AUTHOR(S) (First name, middle initial, last name)

George W. Kattawar
Gilbert N. Plass

6. REPORT DATE	7a. TOTAL NO. OF PAGES	7b. NO. OF REFS
24 August 1967	41	10

8a. CONTRACT OR GRANT NO.	9a. ORIGINATOR'S REPORT NUMBER(S)
AF19(628)-5039 b. PROJECT NO. 4076- 04 c. 62405484 634076	Scientific Report No. 5 9b. OTHER REPORT NO(S) (Any other numbers that may be assigned this report) AFCRL-

10. DISTRIBUTION STATEMENT

Distribution of this document is unlimited. It may be released to the Clearinghouse, Department of Commerce, for sale to the general public.

11. SUPPLEMENTARY NOTES	12. SPONSORING MILITARY ACTIVITY
also by the National Aeronautics and Space Administration contract	Air Force Cambridge Research Laboratories (CRO), L. G. Hanscom Field Bedford, Massachusetts 01730

13. ABSTRACT

The light reflected and transmitted from clouds with various drop size distributions is calculated by a Monte Carlo technique. Six different models are used for the drop size distribution: isotropic; Rayleigh; haze continental; haze maritime; cumulus; nimbostratus. The scattering function for each model is calculated from the Mie theory. In general the reflected and transmitted radiance for the isotropic and Rayleigh models tend to be similar as are those for the various haze and cloud models. The reflected radiance is less for the haze and cloud models than for the isotropic and Rayleigh models, except for an angle of incidence near the horizon when it is larger around the incident beam direction. The transmitted radiance is always much larger for the haze and cloud models near the incident direction; at distant angles it is less for small and moderate optical thicknesses and greater for large optical thicknesses (all comparisons to isotropic and Rayleigh models). The downward flux, cloud albedo, and mean optical path are discussed. The angular spread of the beam as a function of optical thickness is shown for the nimbostratus model.

DD FORM 1 NOV 65 1473

Unclassified
Security Classification